

# Efimov physics in ultracold quantum gases

– *Lecture Notes* –

Richard Schmidt\*

*ITAMP, Harvard-Smithsonian Center for Astrophysics,*

*60 Garden Street, Cambridge, MA 02138, USA and*

*Physics Department, Harvard University,*

*17 Oxford Street, Cambridge, MA 02138, USA*

(Dated: 11-2014)

---

\*Electronic address: richard.schmidt@cfa.harvard.edu

# Part I - Two-body physics and phenomenology of the Efimov effect

## I. INTRODUCTION

As we discussed in the previous lectures dilute vapors of atoms can be confined in magnetic and optical traps. Using various experimental techniques [1] these vapors can then be cooled to extremely low temperatures of  $\mathcal{O}(nK)$ . In terms of absolute temperatures ultracold atoms are among the coolest matter known in nature.<sup>1</sup> With the exception of liquid Helium, at such low temperatures the absolute ground state of the system is a solid and the ultracold gas is therefore in a metastable state. As discussed in previous lectures, the decay of the ultracold vapor towards the solid state takes mainly place due to three-body recombination collisions of atoms. To increase the lifetime of the ultracold atomic samples these processes have to be suppressed which is why the atomic gas has to be made very dilute. Although in consequence the typical interparticle distance  $d$  becomes rather large, it is because of the ultracold temperatures that the thermal de Broglie wavelength of the atoms can by far exceed the interparticle spacing  $d$  and quantum (statistical) effects become relevant. Already here we see that a deep understanding of three-body processes is of great importance to understand the stability of the gas, which applies in particular to situations where strong interactions are involved. But before coming to the physics of three strongly interacting particles, let us briefly review the basics of low energy scattering theory covered in previous lectures. Note that most part of these lecture notes follow closely the excellent review [4] as well as [5].

## II. TWO-BODY PHYSICS AND UNIVERSALITY

Ultracold atoms can be described exceptionally well by theoretical physics for various reasons. Most importantly, the interactions between the atoms can be modeled in very

---

<sup>1</sup> Of course, in relative scales the temperatures are not as cold as they might seem: for instance, in experimentally realizable two-component Fermi gases the Fermi temperature  $T_F$  itself is very low so that the lowest achievable relative temperature  $T/T_F$  is today only on the percent level. This is comparable but not less than what is found in typical metals at room temperature [2] or neutron stars [3].

simple terms although, at first sight, the interaction potential  $V(r)$  of two colliding atoms is rather complicated. In terms of this interaction potential, the corresponding interaction Hamiltonian is given by

$$\hat{H}_{\text{int}} = \int d^3r \int d^3r' \hat{\psi}^\dagger(\mathbf{r}') \hat{\psi}(\mathbf{r}') V(|\mathbf{r} - \mathbf{r}'|) \hat{\psi}^\dagger(\mathbf{r}) \hat{\psi}(\mathbf{r}) \quad (1)$$

with creation and annihilation operators  $\hat{\psi}^\dagger$ ,  $\hat{\psi}$  of bare atoms of mass  $m$  and where at large distances  $r$  the atoms interact via a van-der Waals type potential with a tail  $\sim 1/r^6$  which is a short-range potential [6]. The wave function governing the scattering of two atoms is given by

$$\psi(\mathbf{r}) = e^{ikz} + f_k(\theta) \frac{e^{ikr}}{r}. \quad (2)$$

Here  $\theta$  is the angle between the incoming and outgoing wave vectors while  $k$  is defined by the energy of the incoming particles in the center-of-mass frame,  $E = \hbar^2 k^2 / m$ . For spherical symmetric potentials the scattering amplitude  $f_k(\theta)$  can be expanded in partial waves

$$f_k(\theta) = \sum_{L=0}^{\infty} \frac{2L+1}{k \cot \delta_L(k) - ik} P_L(\cos \theta), \quad (3)$$

where  $L$  denotes the relative angular momentum of the incoming particles. As previously shown, the scattering phases  $\delta_L$  scale as  $\delta_L \sim k^{2L+1}$ . Since the ultralow temperatures of ultracold atoms imply a very small collision energy  $E = \hbar^2 k^2 / m$  of the atoms, the scattering amplitude – which carries the full information about the non-relativistic two-body scattering – is then given by the s-wave channel  $L = 0$ . At these low energies we may further expand the s-wave amplitude  $f(k)$  in  $k$  to obtain

$$f(k) = \frac{1}{-1/a - ik + \frac{r_e}{2} k^2 + \dots} \quad (4)$$

which in terms of the phase shift  $\delta_{L=0}$  corresponds to

$$k \cot \delta_0(k) = -1/a + \frac{r_e}{2} k^2 + \dots. \quad (5)$$

Here  $a$  is the s-wave scattering length while  $r_e$  is called effective range. The effective range  $r_e$  is typically of the order of the true range  $r_0$  of the underlying short-range (single-channel) potential <sup>2</sup>. At very low energies the scattering amplitude then has the very simple (universal)

---

<sup>2</sup> For two-channel models such as employed often in the description of the BEC-BCS crossover the effective range is in fact negative.

form

$$f(k) = \frac{1}{-1/a - ik}. \quad (6)$$

The key to simplicity and an efficient description of ultracold atoms is that the scattering amplitude in Eq. (6) remains exactly the same, no matter which concrete short-range interaction potential is chosen. This applies in particular to the simple contact interaction  $V(r) \sim \delta(r)$  so that ultracold atoms can theoretically be described by the much simpler Hamiltonian

$$\hat{H}_{\text{int}} = g_{\Lambda} \int d^3r \hat{\psi}^\dagger(\mathbf{r}) \hat{\psi}(\mathbf{r}) \hat{\psi}^\dagger(\mathbf{r}) \hat{\psi}(\mathbf{r}). \quad (7)$$

Here, the coupling constant  $g_{\Lambda}$  is chosen such that it yields the desired scattering length  $a$  in Eq. (6). As long as all scales such as temperature, density, a corresponding Fermi energy or binding energies are small, the low-energy limit is justified and the Hamiltonian (7) is a valid representation of the true interaction Hamiltonian (1). In fact here we encounter a simple example of the concept of *universality* which is a guiding principle in the description of systems ranging from few- to many-body physics. Quite generally, a phenomenon is called universal, if the observables are independent of the microscopic details such that the system is characterized by a few variables only. Cold atoms are an example for such a system. In our example of two-body scattering the observable macrophysics, e.g.  $f(k)$ , is independent of the exact realization of the microphysics, that is, the exact form of the potential  $V(r)$ , and it is described in terms of a few relevant parameters only; namely the scattering length  $a$ .<sup>3</sup>

For positive scattering length  $a$ , the scattering amplitude (6) has a pole at  $k = \kappa = i/a$ . This pole corresponds to the presence of a weakly bound state of energy

$$\epsilon_D = \frac{\hbar^2}{ma^2} \quad (a \gg r_0). \quad (8)$$

---

<sup>3</sup> The appearance of universality is intimately related to the existence of renormalization group fixed points [7]. Various theories, although being different on the microscopic level, may flow to the same fixed point and thus, at large distances, lead to the same observable physics. The non-relativistic system of cold atoms is governed by the existence of two fixed points [8]. One is a weak coupling or so-called Gaussian fixed point, the other a strong coupling fixed point which corresponds to unitary interactions. In the context of Bose-Einstein condensation, universality is usually connected to the Gaussian fixed point and is thus a weak coupling phenomenon. In the following we will be interested in the universality associated to the non-perturbative fixed point. Here, the system is characterized by a large scattering length,  $|a| \gg r_0$ , and universality applies as well.

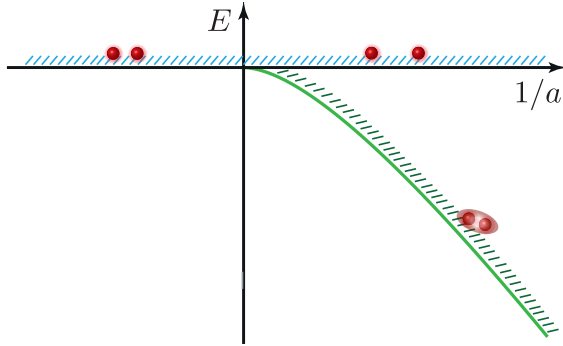


Figure 1: Energy spectrum of two particles interacting resonantly via short range interactions in the limit of large scattering length  $a$ . The atoms can propagate on the scattering threshold at zero energy or form a bound state for positive large scattering lengths. In the universal regime where  $a \gg r_0$  the dimer has a binding energy given by Eq. (8).

This formula is universal and valid for *all* attractive short-range interaction potentials as long as the binding wave vector  $\kappa$  remains small (for an illustration see Fig. 1). Otherwise the expansion in small  $k$  in Eq. (4) breaks down rendering Eq. (8) invalid. This in turn implies that a large (often called resonant) scattering length  $a \gg r_0$  is necessary to reach the regime where this so-called *weakly bound dimer* is present. The real space wave function of the dimer is given by

$$\psi_D(\mathbf{r}) = \frac{1}{r} e^{-r/a} \quad (9)$$

so that its size is roughly given by the scattering length  $a$ . Note that the weakly bound dimer (for its existence the statistics of the two particles involved is irrelevant as long as they are not identical fermions) has been discussed at length in the previous lecture on the BEC-BCS crossover where it represented the molecule leading to the formation of a molecular BEC in the BEC regime of the crossover. In fact, the BEC-BCS crossover is another example of universality: in the unitary limit where the scattering length diverges,  $a \rightarrow \infty$ , the Fermi momentum remains the only length scale in the problem and as long as it is small compared to the range of interactions, universality again applies. For instance the chemical potential of the Fermi gas has been measured to be [9]<sup>4</sup>

$$\mu = \xi \epsilon_F, \quad \xi = 0.376(4), \quad (10)$$

---

<sup>4</sup> An improved experimental analysis of the Feshbach resonance position in the  ${}^6\text{Li}$  Fermi gas yields a corrected value of the Bertsch parameter  $\xi = 0.370(5)(8)$  [10].

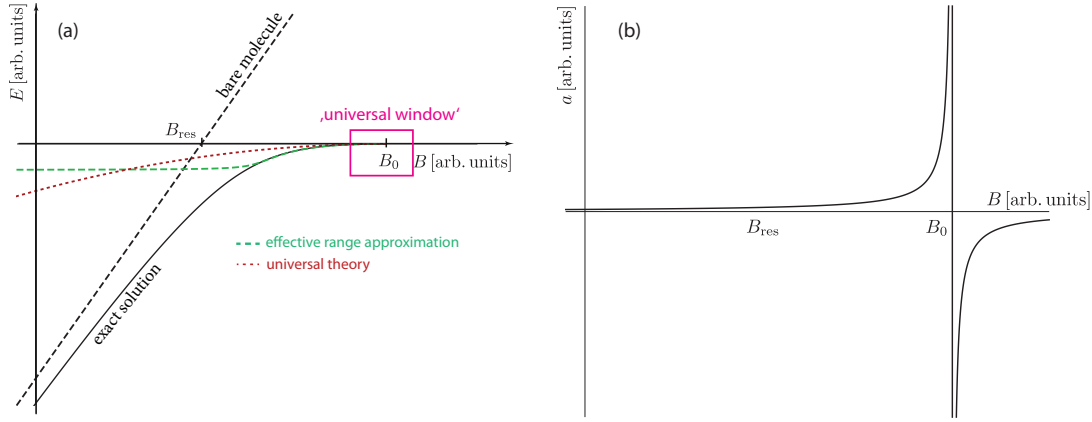


Figure 2: (a) Binding energy spectrum for a realistic two-channel model as employed in the study of the non-universal aspects of Efimov physics in [13]. The universal formula for the dimer binding energy is valid only close to the point where the Feshbach resonance appears and which coincides with the dimer merging into the atom threshold at  $B = B_0$ . Note that effective range description Eq. (12) holds for a much wider range of magnetic fields. (b) Corresponding scattering length dependent on magnetic field.

which is in excellent agreement with theoretical results [11]. Here  $\xi$  is the so-called Bertsch parameter which is a universal number. Similarly, excellent agreement between theory and experiment is found for the critical temperature  $T_c/T_F$ , which is also a universal number. Accordingly, although measured in cold atoms, the same numbers apply to other systems such as neutron stars [12].

### A. Deviations from universality

In the regime of large scattering length (and at low scattering energies)  $a$  is the only parameter in the problem and observables, such as the dimer binding energy are completely universal at low energies. Furthermore physics is termed scale invariant in this regime since observables do not change under a simple rescaling

$$a \rightarrow \lambda a, \quad E \rightarrow \lambda^{-2} E. \quad (11)$$

A simple example is again the dimer binding energy or the scattering cross section.

As one, however, goes away from this regime, so called scaling violations appear. For instance, the effective range becomes relevant in Eq. (4). Another example is the dimer binding energy which changes to

$$\begin{aligned} E_D &= \frac{\hbar^2}{mr_e^2} \left(1 - \sqrt{1 - 2r_e/a}\right)^2 \\ &\approx \frac{\hbar^2}{ma^2} \left(1 + \frac{r_e}{a} + \frac{5r_e^2}{4a^2} + \dots\right). \end{aligned} \quad (12)$$

Thus, if one goes too far away from the resonant limit where  $a \gg r_0$  (or in terms of the effective range  $a \gg |r_e|$ ) scale invariance is violated as well as the universality of observables such as the dimer binding energy. In Fig. 2 we show the dimer binding energy in a two-channel model (discussed in previous lectures) as function of the magnetic field. As one can see the universal formulas apply only in a rather narrow window of magnetic field. Away from that regime non-universal corrections such as in Eq. (12) become relevant.

### III. EFIMOV PHYSICS - PHENOMENOLOGY

So far we have discussed the physics of two particles interacting resonantly via a short range potential at very low scattering energies (from now on we will consider – with very few exceptions – exclusively interacting bosons). The energy spectrum, shown in Fig. 1, turns out to be very simple. The two atoms can either form a bound state (green solid line) with universal binding energy (8) or propagate freely on the scattering threshold at zero energy (blue hatched line).

When three identical bosons interact with resonant short-range potentials ( $a \gg r_0$ ) a new universal quantum phenomenon is revealed. This was first realized by Vitaly Efimov in 1970 when solving exactly the quantum three-body problem. Efimov showed the existence of a series of *infinitely* many three-body bound states in the resonance limit,  $a \rightarrow \infty$  [14].<sup>5</sup> The binding energies of the so-called Efimov trimers form a geometric spectrum so that the binding energies of consequent levels exhibit a constant ratio<sup>6</sup>

$$\frac{E_{n+1}^T}{E_n^T} = e^{\frac{2\pi}{s_0}} = 515.03\dots, \quad s_0 = 1.00624\dots \quad (13)$$

---

<sup>5</sup> The Efimov effect occurs quite generally if two out of three pairs of the participating particles are interacting with a large scattering length [4].

<sup>6</sup> Here the universal number  $s_0$  is given for the case of identical bosons.

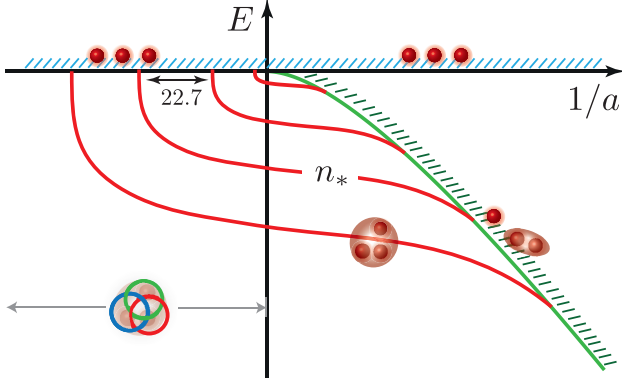


Figure 3: Illustration of the Efimov energy spectrum. The Efimov trimers (red solid) extend from the atom threshold (blue hatching) at vanishing energy  $E = 0$  and  $a < 0$  to the side of positive scattering length  $a > 0$  where they merge into the atom-dimer threshold (green solid). For negative  $a$ , the trimers are of Borromean nature as they exist in a regime where no two-body bound state exist – a purely quantum phenomenon not present in classical mechanics. Note that we have rescaled the axis to make several of the Efimov states visible — we used the ‘traditional’ method to plot  $|E|^{1/4}$  versus  $\text{sign}(a)|a|^{-1/4}$ .

when the *unitarity point*  $1/a = E = 0$  is approached. As discussed above, at this point two bosons are just at the verge of being bound into the weakly bound dimer. Below we will explicitly verify (13) using a quantum mechanical calculation.

In Fig. 3 we show a typical Efimov bound state spectrum where the axis are rescaled in order to make several of the three-body bound states visible. Each of the infinitely many Efimov states evolves from the three-atom threshold (dashed blue hatching) for  $a < 0$  across the resonance and merges into the atom-dimer scattering threshold for  $a > 0$  (green line). Quite counterintuitively, the trimer states exist even in a regime where no two-body bound state is present. In this regime the Efimov states are sometimes called Borromean in reference to the family seal of a legendary Italian family which shows three rings entangled in such a way that if one takes one of the three away and the whole system falls apart.

Eq. (13) is a universal law as it does not depend on any short-range details. The only important ingredients are: short-range interactions, a large scattering length  $|a| \gg r_0$ , and energies  $|E| \ll \hbar^2/(mr_0^2)$ . It was predicted by Efimov in the context of nuclear physics and it took more than thirty years to find experimental evidence for its existence. Its observation is an example of the broad implications of universality: instead of being found in a nuclear

system, the Efimov effect was observed using ultracold atoms close to a Feshbach resonance [15]. Unfortunately, the search for Efimov states in the nuclear matter context has been quite unsuccessful so far, as well as the search for a predicted  ${}^3\text{He}$  trimer despite decades of research devoted to the search for this elusive trimer [16, 17].

The Efimov effect, whose existence was rigorously proven by Amado and Noble [18, 19], demands the introduction of a new notion of universality. Although the existence of the Efimov states, the relation (13), as well as the shape of the spectrum shown in Fig. 3 is universal, the absolute value of the binding energies, that is the actual position of the set of states, is not universally fixed. In fact, the whole Efimov spectrum in Fig. 3 can be shifted arbitrarily while leaving universal ratios such as Eq. (13) unaffected. This arbitrariness necessitates the introduction of an additional *three-body parameter* (3BP). This is made explicit by rewriting the Efimov binding energies as [4]

$$E_T^{(n)} = \left( \frac{1}{515.03} \right)^{n-n^*} \frac{\hbar^2 \kappa_*^2}{m}, \quad (14)$$

where  $n^*$  denotes the number of some ‘reference Efimov state’ as indicated in Fig. 3. The wave number  $\kappa_*$  is a free parameter which is chosen to set the overall position of the spectrum.  $\kappa^*$  can be regarded as the three-body parameter but this is not a unique choice. From Fig. 3 it is evident that one may choose any observable which fixes the overall position of the spectrum. This could, for instance, also be the value of the scattering length  $a_-^{(n^*)} < 0$ , where the reference trimer  $n^*$  meets the three-atom threshold. As shown by Efimov, the trimers meet the atom threshold at values [20]

$$a_-^{(n)} = 22.6942^{n-n^*} a_-^{(n^*)}, \quad (15)$$

for large  $|a|/r_0 \gg 1$ .

Due to the Efimov effect, two-body universality is violated: not only the scattering length  $a$  is needed in order to characterize the physics but an additional parameter. While in the two-body problem non-universal corrections scale as positive powers of  $r_0/|a|$  and hence are suppressed for large  $|a|$ , the three-body parameter  $\kappa^*$  never disappears. It reflects the ignorance of the short-range details of the interatomic potentials and thus it had – until recently – been regarded as a non-universal number.

### A. Unitary and zero-range limit

From Efimov's results (13) and (14) it follows that there are infinitely many *weakly* bound trimers. But how does the spectrum behave for the *deeply* bound states? In order to answer this question let us define two important limits. We argued that non-universal corrections to the two-body scattering scale as powers of  $r_0/|a|$ . There are two limits in which these corrections go to zero. One is the so-called:

#### ***Unitary or resonance limit [4]***

$$|a| \rightarrow \infty, \quad r_0 \text{ finite.} \quad (16)$$

In this limit infinitely many, *weakly* bound trimer states exist. One can go away from the resonance limit by lowering the absolute value of the scattering length  $|a|$ . When the inverse wavenumber of the  $n$ th bound state  $1/\kappa^{(n)}$  or the corresponding scattering length  $a_-^{(n)}$ , where it meets the atom threshold, becomes of order  $r_0$ , the Efimov states cease to exist due to the finite range of the interaction potentials. Hence there will be a *lowest* Efimov state. The Efimov states in this situation are illustrated as solid red lines in Fig. 4. As also indicated, the low-lying states can not be expected to obey the universal geometric scaling, since here non-universal corrections of order  $r_0/|a|$  become relevant. For this reason one expects that

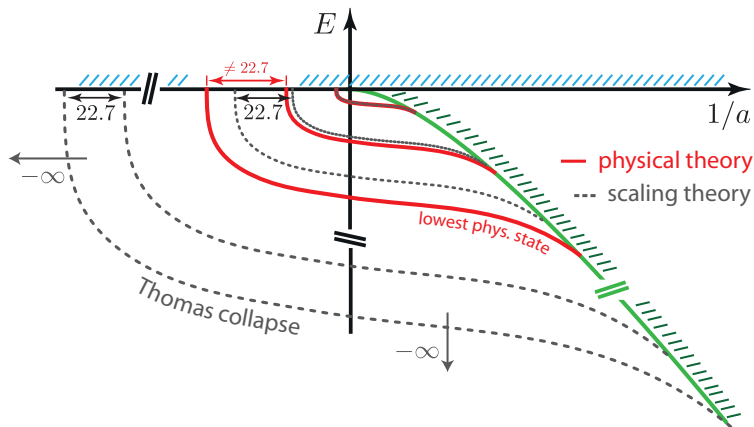


Figure 4: Illustration of the Efimov spectrum obtained from scaling theory (dashed black) compared to a (physical) finite range model (solid red).

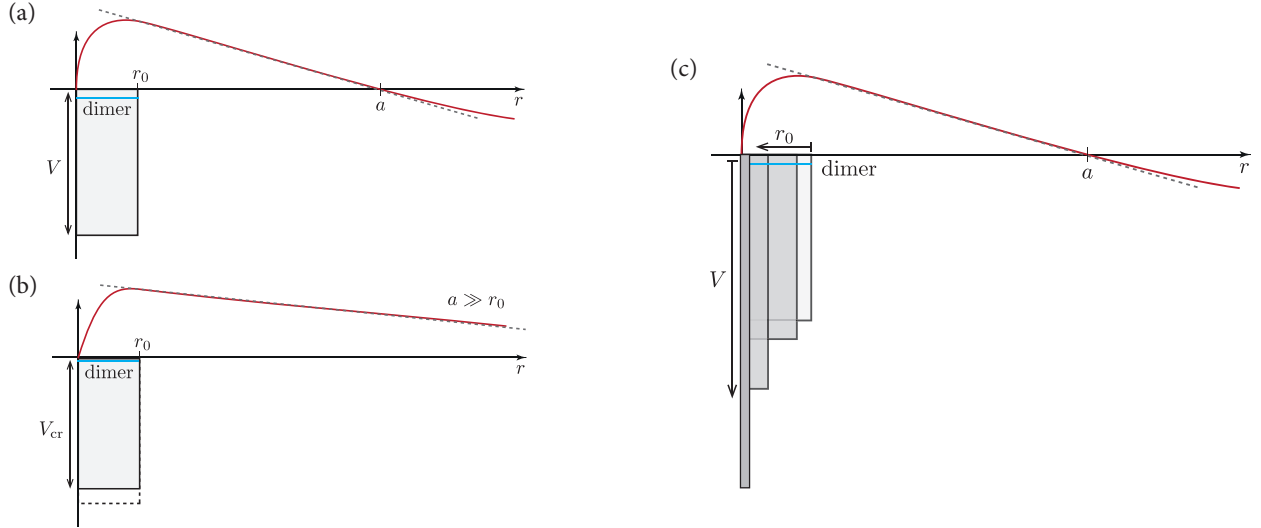


Figure 5: (a) and (b): Shape resonance. The depth of a square well potential is fine-tuned to a critical value where the scattering length diverges and the weakly bound molecule disappears into the scattering continuum. (c) Zero-range limit. While keeping the scattering length  $a$  fixed, the range of the potential is sent to zero. In (a-c) also the wave function, which defines the scattering length  $a$ , is indicated as red solid line.

the specific position of the lowest state is highly dependent on microscopic details. This explains why the three-body parameter is expected to be a non-universal number.

The resonance limit is a very physical limit and it can be realized using a shape resonance as depicted in Fig. 5(a) and (b) for the case of a square well potential. Keeping the potential range constant, the depth of the potential is fine-tuned to a critical value  $V_{\text{cr}}$  at which a two-body bound state just vanishes into the continuum. Another possibility to reach the resonance limit is the use of Feshbach resonances discussed in previous lectures. Note, however, that in the end, as long as we are only interested in the regime of large scattering length and energies close to zero, it does not matter which model we use to achieve this regime: the scattering amplitude Eq. (6) will always be the same.

The second limit in which the corrections  $r_0/|a|$  go to zero is the

#### **Zero-range or scaling limit [4]**

$$|a| \text{ fixed}, \quad r_0 \rightarrow 0. \quad (17)$$

This limit is illustrated in Fig. 5(c). In this limit, which is often referred to as scaling limit, the purely theoretical, idealized situation of contact interactions is realized and the two-particle interaction potential reads  $V(\mathbf{r}' - \mathbf{r}) = g\delta(\mathbf{r}' - \mathbf{r})$ . The scattering phase shift becomes exactly  $k\cot\delta_0(k) = -1/a$  for the partial s-wave and vanishes identically for all higher partial waves,  $\delta_L \equiv 0$  for  $L > 0$ . At first sight the zero-range limit seems quite unphysical, as realistic interaction potentials always have a finite range. The non-universal corrections due to the true physical range vanish, however, as powers of  $r_0/|a|$  so that in the limit of large scattering length the scaling limit yields accurate results. The zero-range limit has the advantage that it makes calculations feasible and we will use it in our following quantum mechanical derivation of the Efimov effect.

As soon as  $|a|$  or the relevant, inverse wave numbers  $1/\kappa$  become of order of  $r_0$ , the scaling limit leads to unphysical or even pathological results. For instance, it predicts that there are not only infinitely many weakly bound trimer states but also infinitely many *infinitely deeply* bound states. The reason for this pathological behavior is the absence of any scale  $r_0$  which prevents the system from collapsing to infinite binding energies - and thus the collapse of the trimers to infinitely small size. Obviously this collapse is prevented in nature by the presence of a finite potential range and, theoretically, it is prevented by the presence of a regulating effective range term  $\sim r_e k^2/2$  in the inverse scattering amplitude  $f(k)$ . Furthermore, due to the absence of any short-range scale, *all* Efimov states exactly obey the universal scaling relations such as Eqn. (14) and (15). The corresponding Efimov states are illustrated as dotted lines in Fig. 4. However, the dependence on the three-body parameter  $\kappa^*$ , cf. Eq. (14), is still present, and  $\kappa^*$  has to be fixed to determine the overall position of the spectrum. It is of importance – and unfortunately often not properly taken into account in the literature – to realize that the scaling limit only leads to valid predictions when  $|a|$  is *much* larger than the range  $r_0$ . Since so far in experiments only the lowest, deep Efimov states are accessible, this regime is typically not realized, and thus, strictly speaking, scaling theory *cannot* be applied.

The collapse of the trimer states to infinite binding energies is connected to what was found by Thomas prior to the calculation by Efimov [21]. He considered atoms interacting via a square well potential where he performed the scaling limit  $r_0 \rightarrow 0$  while keeping  $a$  constant, cf. Fig. 5 (c). He showed that there exists a three-body bound state with binding energy  $E_{\text{tri}} \sim -\hbar^2/(mr_0^2) \rightarrow -\infty$ . In 1979, Efimov succeeded to connect Thomas' and his

own work and showed that there are the above mentioned infinitely many, deep trimer states where the deepest of those scales as  $E_{\text{tri}} \sim -\hbar^2/(mr_0^2) \rightarrow -\infty$  [20].

### B. Side remark: Efimov effect and the renormalization group.

The Efimov effect also leaves its traces in a renormalization group analysis of the three-body problem. It represents one of the extremely rare cases where a renormalization group limit cycle [22] is realized in nature.

As mentioned before, the two-body sector is governed by a strong coupling fixed point [7]. The existence of the fixed point directly implies that the system exhibits scale invariance so that the system is invariant under the *continuous* scale transformations, cf. Eq. (11)

$$a \rightarrow \lambda a \quad \mathbf{r} \rightarrow \lambda \mathbf{r} \quad t \rightarrow \lambda^2 t. \quad (18)$$

The Efimov effect changes the situation. One finds that the running of the three-body coupling exhibits a flow which is log-periodic in the RG momentum scale  $k$  as shown in Fig. 6(a). The periodicity of the flow is given by the Efimov number  $s_0$ , which Efimov showed to obey [14] (below we will explicitly derive this equation)

$$s_0 \cosh \frac{\pi s_0}{2} = \frac{8}{\sqrt{3}} \sinh \frac{\pi s_0}{6}. \quad (19)$$

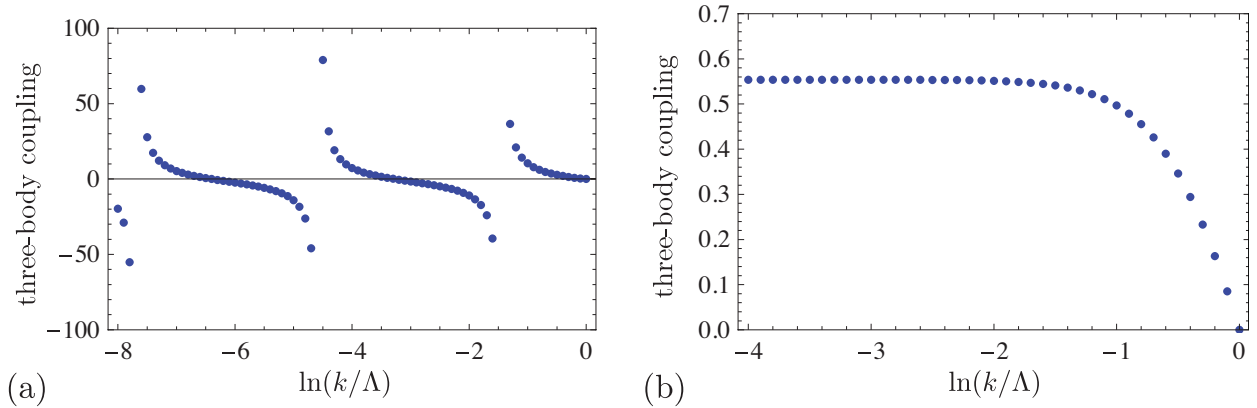


Figure 6: Renormalization group flow of the three-body coupling constant with logarithmic RG scale  $k$  in units of the UV cutoff scale  $\Lambda$  as computed in [23] for (a) bosons, (b) SU(2) fermions.

The log-periodic structure of the limit cycle flow reflects the geometric spectrum (14): when the RG scale is changed by a multiple factor of  $\exp(\pi/s_0)$  new divergencies appear in the flow of the three-body coupling and these divergencies correspond to the appearance of new bound states. The three-body parameter  $\kappa_*$  also appears in the renormalization group framework and it sets the overall phase of the renormalization group flow. In a sense [4],  $\kappa_*$  labels a continuous set of universality classes. The periodic structure of the flow with its fixed frequency  $\pi/s_0$  reveals that the continuous scale invariance present in the two-body problem is broken and only a *discrete scale invariance* remains. This symmetry breaking is purely quantum, and one may speak of a quantum anomaly. The system is now invariant only under the discrete scale transformations:

$$\kappa_* \rightarrow \kappa_* \quad a \rightarrow \lambda_0^n a \quad \mathbf{r} \rightarrow \lambda_0^n \mathbf{r} \quad t \rightarrow \lambda_0^{2n} t$$

with

$$\lambda_0 = e^{\pi/s_0}. \quad (20)$$

It is worth mentioning that scale invariance is a very important feature when considering many-body systems such as the unitary Fermi gas [11]. It allows to derive many exact relations such as the vanishing of the bulk viscosity [24] or the exact time evolution of the system [25]. Contrarily, if one considers unitary bosons, scale invariance is broken, rendering calculations much more difficult. For two-component fermions with a mass-imbalance smaller than a factor of 13.6 [26] no Efimov effect, however, takes place. Instead of showing a periodic limit cycle the atom-dimer coupling exhibits an RG fixed point tied to the renormalization group running of the two-body sector, cf. Fig. 6(b). Thus scale invariance is preserved, and calculations can safely exploit this important symmetry.

## Part II - Quantum mechanical derivation and observation of the Efimov effect

In the following we will derive the Efimov effect in the scaling limit and show the existence of the geometric scaling of the Efimov spectrum. There is a plethora of methods for dealing with this kind of few-body problems ranging from standard quantum wave mechanics [27] to effective field theory [4] to field-theoretical renormalization group methods [28]. While ‘first quantization’ methods are most suited when dealing with the question of the influence of microscopical details on the Efimov physics away from unitarity, RG techniques have the advantage to allow to address questions of few- and many-body physics within one framework. For this lecture we will take the original quantum mechanical approach to the problem. This approach has also the advantage of allowing to address directly the structure of the three-body wave function in *coordinate space* while quantum field theory approaches typically work in momentum space which renders the physical interpretation of some results more difficult. In this part of the lecture we follow very closely the excellent review by Braaten and Hammer [4].

### IV. JACOBI AND HYPERSPHERICAL COORDINATES

We consider the quantum mechanical problem of three particles interacting via short-range interactions. For simplicity we assume a system of three bosons of equal mass  $m$ . The Schrödinger equation for the three particles is given by

$$\left(-\frac{\hbar^2}{2m} \sum_{i=1}^3 \nabla_i^2 + V(\mathbf{r}_1, \mathbf{r}_2, \mathbf{r}_3)\right) \Psi(\mathbf{r}_1, \mathbf{r}_2, \mathbf{r}_3) = E\Psi(\mathbf{r}_1, \mathbf{r}_2, \mathbf{r}_3). \quad (21)$$

For a translationally invariant system a center of mass frame can be defined <sup>7</sup> and the wave function depends only on six independent variables.

An important step towards a solution is a deliberate choice of coordinates. This is done in two steps: First we introduce the Jacobi coordinates. From those one can derive hypercoordinates which will simplify the calculation considerably.

---

<sup>7</sup> In cases where, for instance, the particles are confined, or if a spin orbit coupling is present, such a separation is not possible. The problem then becomes decisively more complicated and has, to our knowledge, up to now not been solved.

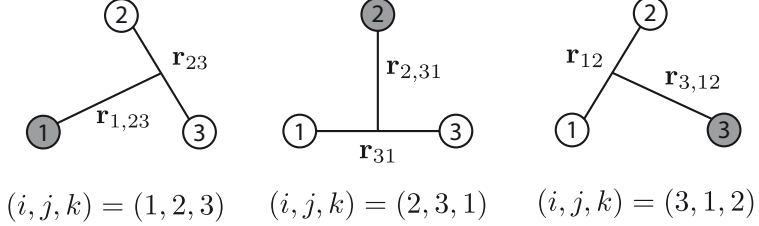


Figure 7: Illustration of the Jacobi coordinates. There are three distinct, but equivalent set of Jacobi coordinates. To each set belong two vectors  $\mathbf{r}_{jk}$  and  $\mathbf{r}_{i,jk}$ . Since each set consists of 6 independent variables they suffice to characterize the three-body system completely.

The Jacobi coordinates are defined by

$$\mathbf{r}_{i,jk} = \mathbf{r}_i - \frac{1}{2}(\mathbf{r}_j + \mathbf{r}_k), \quad \mathbf{r}_{jk} = \mathbf{r}_j - \mathbf{r}_k. \quad (22)$$

As illustrated in Fig. 7, there are three equivalent sets of Jacobi coordinates. Each set corresponds to one of the three possible choices of a ‘reference’ atom which is denoted by the index  $i$  in the equation above (gray atom in the Fig. 7). For instance, in the left set of Fig. 7 the set with indices  $(i, j, k) = (1, 2, 3)$  is chosen.

The next step is to introduce ‘space-fixed’ hyperspherical coordinates. The *hyperradius* is given by

$$R^2 = \frac{1}{3}(r_{12}^2 + r_{23}^2 + r_{31}^2) = \frac{1}{2}r_{jk}^2 + \frac{2}{3}r_{i,jk}^2. \quad (23)$$

It is a measure for the (root-mean square) size of the three-body system. For a given set of Jacobi coordinates one defines the hyperangle  $\alpha_i$  by

$$r_{jk} \equiv |\mathbf{r}_{jk}| = \sqrt{2}R \sin \alpha_i, \quad (24)$$

$$r_{i,jk} \equiv |\mathbf{r}_{i,jk}| = \sqrt{3/2} R \cos \alpha_i. \quad (25)$$

Thus  $\alpha_i$  can be expressed as

$$\alpha_i = \arctan \left( \frac{\sqrt{3}r_{jk}}{2r_{i,jk}} \right). \quad (26)$$

This formula makes apparent that the hyperangle  $\alpha_i$  determines the relative size of the vectors  $\mathbf{r}_{jk}$  and  $\mathbf{r}_{i,jk}$ . The hyperangle ranges from  $0 \dots \pi/2$ .<sup>8</sup> The significance of the hyperangle

<sup>8</sup> The hyperangles of the different Jacobi sets are related via the formula

$$\sin^2 \alpha_j = \frac{1}{4} \sin^2 \alpha_i + \frac{3}{4} \cos^2 \alpha_i + \frac{1}{2} \sqrt{3} \sin \alpha_i \cos \alpha_i \hat{\mathbf{r}}_{jk} \cdot \hat{\mathbf{r}}_{i,jk}, \quad (27)$$

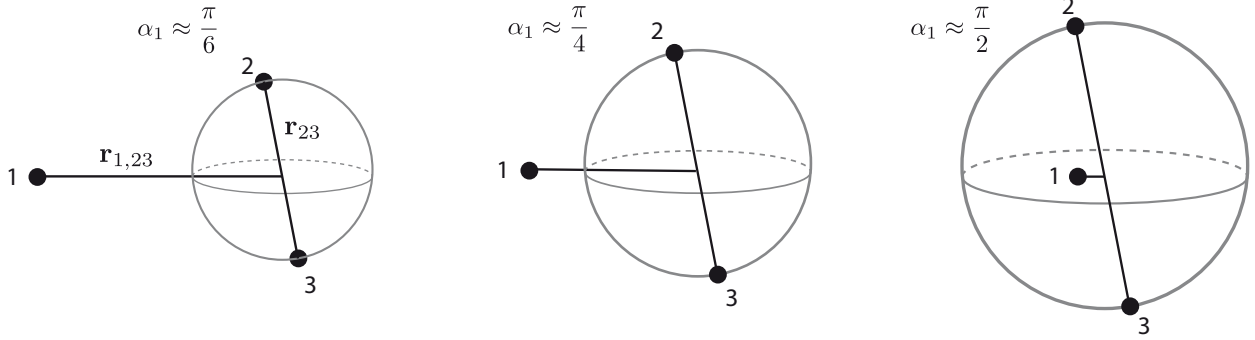


Figure 8: Illustration of the hyperangle  $\alpha_i$ . Throughout this figure the set of Jacobi coordinates with  $i = 1$  is chosen. Each of the configuration corresponds to the same hyperradius  $R$ . The hyperangle  $\alpha_1$  increases from the left to right. The sphere indicates that for fixed hyperangle  $\alpha_1$  the two atoms 1 and 2, which are connected via the vector  $\mathbf{r}_{23}$ , can be rotated to any position on the sphere while keeping  $R$  and  $\alpha_1$  constant. The smaller  $\alpha_1$  the closer the atoms  $j = 2$  and  $k = 3$  are together (left). On the other hand as  $\alpha_1$  approaches the limiting value  $\pi/2$  atoms 2 and 3 move away from each other until the exhaust the hyperradius given by Eq. (23) (right figure). Then  $\alpha_1 = \pi/2$  and the atom 1 is forced to be situated exactly in the middle of atoms 2 and 3.

$\alpha_i$  is illustrated in Fig. 8. In this figure the set of Jacobi coordinates with  $i = 1$  is chosen. Each of the configuration corresponds to the same hyperradius  $R$  while the hyperangle  $\alpha_1$  increases from the left to right. The sphere indicates that for fixed hyperangle  $\alpha_1$  the two atoms 1 and 2, which are connected via the vector  $\mathbf{r}_{23}$ , can be rotated to any position on the sphere while keeping  $R$  and  $\alpha_1$  constant. The minimal  $\alpha_{i=1} = 0$  is achieved when the atoms  $j = 2$  and  $k = 3$  are on top of each other. Then  $\mathbf{r}_{jk} = 0$  while  $\mathbf{r}_{i,jk}$  reaches its maximal length given by  $r_{i,jk}^2 = 3/2R^2$ , cf. Eq. (23). On the other hand  $\alpha_i = \pi/2$  corresponds to the situation where the atoms  $j$  and  $k$  have maximal separation (see Fig. 8(right)) allowed by a given hyperradius. Then the ‘reference’ atom  $i$  is situated in the middle of atoms  $j$  and  $k$ .

The set of hyperspherical coordinates is completed by additionally choosing the angles characterizing the angular orientations of the unit vectors  $\hat{\mathbf{r}}_{i,jk}$  and  $\hat{\mathbf{r}}_{jk}$  (denoted by  $\Omega_{i,jk}$  and  $\Omega_{jk}$ , respectively) as further coordinates. This determines the set of hyperspherical

---

where  $(i, j, k)$  is a permutation of  $(1, 2, 3)$ .  $\hat{\mathbf{r}}_{i,jk}$  and  $\hat{\mathbf{r}}_{jk}$  denote the unit vectors of the respective Jacobi coordinate vectors.

coordinates which are given by

$$\text{hyperspherical coordinates: } (R, \underbrace{\alpha_i, \Omega_{i,jk}, \Omega_{jk}}_{\Omega}). \quad (28)$$

Here we defined the hyperangular variable  $\Omega = (\alpha_i, \Omega_{i,jk}, \Omega_{jk})$  as a collective index. Hyperspherical coordinates are convenient for two major reasons: First only one variable, namely the hyperradius  $R$  carries a dimension (length). Second the angular variables  $\Omega_{i,jk}$  and  $\Omega_{jk}$  give direct access to the corresponding angular momenta of the system of particles which is important for the simplification of the further analysis.<sup>9</sup>

Finally using involved coordinate transformation rules for the gradient operators [27] it can be shown that the three-body Schrödinger equation in terms of the new hyperspherical coordinates reads

$$\underbrace{\left[ -\frac{\hbar^2}{2m} \left( \frac{\partial^2}{\partial R^2} + \frac{5}{R} \frac{\partial}{\partial R} \right) \right]}_{T_R} - \underbrace{\left[ \frac{\hbar^2}{2mR^2} \left( \frac{\partial^2}{\partial \alpha_i^2} + 4 \cot(2\alpha_i) \frac{\partial}{\partial \alpha_i} \right) \right]}_{T_{\alpha_i}} + \frac{\Lambda_{i,jk}^2}{2mR^2} + V(R, \Omega) \Psi(R, \Omega) = E \Psi(R, \Omega) \quad (30)$$

$$+ \frac{\Lambda_{i,jk}^2}{2mR^2} + V(R, \Omega) \Big] \Psi(R, \Omega) = E \Psi(R, \Omega) \quad (31)$$

with

$$\Lambda_{i,jk}^2 = \frac{\mathbf{L}_{jk}^2}{\sin^2 \alpha_i} + \frac{\mathbf{L}_{i,jk}^2}{\cos^2 \alpha_i}, \quad (32)$$

where  $\mathbf{L}_{jk}$  and  $\mathbf{L}_{i,jk}$  denote the conventional angular momenta corresponding to the motion of the ‘subsystem’ vectors  $\mathbf{r}_{i,jk}$  and  $\mathbf{r}_{jk}$  respectively.

## V. LOW-ENERGY FADDEEV EQUATION

In the following we present a derivation of a single *low-energy* Faddeev equation which will enable us to recover the Efimov effect in the scaling limit including its geometric spectrum

---

<sup>9</sup> Expressed in terms of the hyperspherical coordinates the integral measure can be shown (see e.g. [27]) to transform according to

$$\begin{aligned} d^3 r_{jk} d^3 r_{i,jk} &= \frac{3\sqrt{3}}{4} R^5 dR \sin^2(2\alpha_i) d\alpha_i d\Omega_{jk} d\Omega_{i,jk} \\ &\equiv \frac{3\sqrt{3}}{4} R^5 dR d\Omega. \end{aligned} \quad (29)$$

[29]. First we make the simplifying assumption that the particles' interaction  $V(\mathbf{r}_1, \mathbf{r}_2, \mathbf{r}_3)$  can be separated into a sum of pairwise interactions  $V(r_{ij})$  which are spherically symmetric. For the case of ultracold atoms this is an excellent approximation since three-body forces, such as the Axilrod-Teller potential, are expected to play a minor role (the formalism can, however, be extended to include explicit three-body forces, cf. [27]). The potential then reads

$$V(\mathbf{r}_1, \mathbf{r}_2, \mathbf{r}_3) = V(r_{12}) + V(r_{23}) + V(r_{31}). \quad (33)$$

The Faddeev equations generate solutions of the three-body Schrödinger equation of the form

$$\Psi(\mathbf{r}_1, \mathbf{r}_2, \mathbf{r}_3) = \psi^{(1)}(\mathbf{r}_{23}, \mathbf{r}_{1,23}) + \psi^{(2)}(\mathbf{r}_{31}, \mathbf{r}_{2,31}) + \psi^{(3)}(\mathbf{r}_{12}, \mathbf{r}_{3,12}), \quad (34)$$

and they are given by

$$\left( T_R + T_{\alpha_1} + \frac{\Lambda_{1,23}^2}{2mR^2} \right) \psi^{(1)} + V(r_{23}) (\psi^{(1)} + \psi^{(2)} + \psi^{(3)}) = E\psi^{(1)}, \quad (35)$$

together with the two equations obtained by cyclic permutation of (1, 2, 3). Indeed, upon insertion one can show that the wave function (34) solves Eq. (31) when Eq. (35) is fulfilled. Hence, if one is able to solve the set of equations (35), one has solved the quantum mechanical three-body problem.<sup>10</sup>

The Jacobi vectors  $\mathbf{r}_{i,jk}$  and  $\mathbf{r}_{jk}$  have corresponding angular momentum operators  $\mathbf{L}_{jk}$  and  $\mathbf{L}_{i,jk}$  in the Schrödinger/Faddeev equations. We exploit this fact by decomposing each of the Faddeev wave functions in their respective spherical harmonics. For instance,

$$\psi^{(1)}(\mathbf{r}_{23}, \mathbf{r}_{1,23}) = \sum_{l_x, m_x} \sum_{l_y, m_y} f_{l_x m_x, l_y m_y}^{(1)}(R, \alpha_1) Y_{l_x m_x}(\hat{\mathbf{r}}_{23}) Y_{l_y m_y}(\hat{\mathbf{r}}_{1,23}), \quad (36)$$

where the expansion is with respect to the angular variables  $\Omega_{23}$  and  $\Omega_{1,23}$  in  $\psi^{(1)}(\mathbf{r}_{23}, \mathbf{r}_{1,23}) = \psi(R, \alpha_1, \Omega_{23}, \Omega_{1,23})$ .

The corresponding angular momenta of the subsystems given by the motion of  $\mathbf{r}_{23}$  and  $\mathbf{r}_{1,23}$  come at a cost of kinetic energy. Since we want, however, to address only the low-energy part of the spectrum we may drop all terms but  $l_x = l_y = 0$ . As we will see below,

---

<sup>10</sup> There are non-trivial solutions to the Faddeev equations which correspond to a trivial solution of the three-body Schrödinger equation, when  $\psi^{(1)} + \psi^{(2)} + \psi^{(3)} = 0$ . These solutions are unphysical.

the  $L = 0$  partial wave channel is responsible for the Efimov effect and the appearance of the three-body bound states.

Due to this ‘projection’ onto zero angular momenta, the Faddeev wave functions become independent of the orbital angles  $\Omega_{23}$  and  $\Omega_{1,23}$  and we define

$$\psi^{(1)}(R, \alpha_1) \equiv f_{00}^{(1)}(R, \alpha_1) \quad (37)$$

so that the Faddeev equations become

$$(T_R + T_{\alpha_1} - E) \psi(R, \alpha_1) + V(\sqrt{2}R \sin \alpha_1) \underbrace{[\psi(R, \alpha_1) + \psi(R, \alpha_2) + \psi(R, \alpha_3)]}_{(*)} = 0, \quad (38)$$

together with the two equations resulting from cyclic permutations of  $(1, 2, 3)$  and where we have used the definition in Eq. (25).

So far the Faddeev equations depend on all three hyperangles  $\alpha_i$  which are interrelated through Eq. (27). The goal is now to express the three Eqs. (38) in terms of only one angular variable, e.g.  $\alpha_1$  (from now on we will use  $\alpha \equiv \alpha_1$ ). In order to do so, we have to “rotate” the part denoted by  $(*)$  in Eq. (38) to the first set of Jacobi coordinates and similar in the other two Faddeev equations. This is achieved by taking angular averages of the Faddeev equations over the angles given by the unit vectors  $\hat{\mathbf{r}}_{i,jk}$  and  $\hat{\mathbf{r}}_{jk}$ . As shown by Vinitskii et al. the averages of  $\psi(R, \alpha_2)$  and  $\psi(R, \alpha_3)$  can be expressed as [30]

$$\langle \psi(R, \alpha_2) \rangle_{\hat{\mathbf{r}}_{1,23}, \hat{\mathbf{r}}_{23}} = \langle \psi(R, \alpha_3) \rangle_{\hat{\mathbf{r}}_{1,23}, \hat{\mathbf{r}}_{23}} = \frac{2}{\sqrt{3}} \int_{\pi/3-\alpha}^{\pi/2-|\pi/6-\alpha|} d\alpha' \frac{\sin(2\alpha')}{\sin(2\alpha)} \psi(R, \alpha'). \quad (39)$$

One then arrives at three identical copies of the set of Faddeev equations which read

$$(T_R + T_\alpha - E) \psi(R, \alpha) = -V(\sqrt{2}R \sin \alpha) \times \left[ \psi(R, \alpha) + \frac{4}{\sqrt{3}} \int_{\pi/3-\alpha}^{\pi/2-|\pi/6-\alpha|} \frac{\sin(2\alpha')}{\sin(2\alpha)} \psi(R, \alpha') d\alpha' \right]. \quad (40)$$

This is the *low-energy Faddeev equation* [31].

### A. Solution of the low-energy Faddeev equation

We follow now a strategy similar to the solution of central potential problems where one aims for a separate solution of the angular and radial part of the problem. Following this strategy we expand the Faddeev wave functions  $\psi(R, \alpha)$  for given hyperradius  $R$  in a

complete basis of functions  $\phi_n(R, \alpha)$  which are functions of  $\alpha$  but where  $R$  is treated as parameter. The expansion reads<sup>11</sup>

$$\psi(R, \alpha) = \frac{1}{R^{5/2} \sin(2\alpha)} \sum_n f_n(R) \phi_n(R, \alpha). \quad (41)$$

The angular functions  $\phi_n(R, \alpha)$  are chosen to be the solutions of the ‘angular’ Faddeev equations:

$$\begin{aligned} \left[ -\frac{\partial^2}{\partial \alpha^2} - \lambda_n(R) \right] \phi_n(R, \alpha) &= -\frac{2mR^2}{\hbar^2} V(\sqrt{2}R \sin \alpha) \\ &\times \left[ \phi_n(R, \alpha) + \frac{4}{\sqrt{3}} \int_{|\frac{1}{3}\pi-\alpha|}^{\frac{1}{2}\pi-|\frac{1}{6}\pi-\alpha|} \phi_n(R, \alpha') d\alpha' \right]. \end{aligned} \quad (42)$$

We emphasize again that the hyperradius  $R$  is treated as a parameter and the eigenvalues  $\lambda_n = \lambda_n(R)$  of this differential-integro equation are functions of this parameter.

As a next step we aim to derive an equation for the determination of the radial wave functions  $f_n$ . In order to do, so we insert Eq. (41) into the low-energy Faddeev equation (40). The  $\phi_n$  are projected out via an integration over  $\int d\alpha \phi_n^*(R, \alpha)$ . At this point the derivation of the radial equation differs somewhat from the usual strategy used, for instance, in the solution of the hydrogen atom: Being acted upon by an integro-differential operator the functions  $\phi_n(R, \alpha)$  in Eq. (42) do not have to form a orthogonal set of functions. Therefore the inner product

$$G_{nm}(R) = \int_0^{\frac{\pi}{2}} d\alpha \phi_n^*(R, \alpha) \phi_m(R, \alpha), \quad (43)$$

is not necessarily given by a delta function  $\delta_{nm}$  and the matrix  $G_{nm}$  has to be carried along in the calculation. One finally obtains the radial equation

$$\begin{aligned} \left[ \frac{\hbar^2}{2m} \left( -\frac{\partial^2}{\partial R^2} + \frac{15}{4R^2} \right) + V_n(R) \right] f_n(R) \\ + \sum_m \left[ 2P_{nm}(R) \frac{\partial}{\partial R} + Q_{nm}(R) \right] f_m(R) = E f_n(R), \end{aligned} \quad (44)$$

with  $R$ -dependent coupling potentials  $P_{mn}(R)$  and  $Q_{mn}(R)$  defined by

$$P_{nm}(R) = -\frac{\hbar^2}{2m} \sum_k G_{nk}^{-1}(R) \int_0^{\frac{\pi}{2}} d\alpha \phi_k^*(R, \alpha) \frac{\partial}{\partial R} \phi_m(R, \alpha), \quad (45)$$

---

<sup>11</sup> The prefactor  $1/\sin(2\alpha)$  has been conveniently chosen to impose the boundary condition  $\phi_n(R, \alpha) = 0$  for  $\alpha = 0, \pi/2$ .

and

$$Q_{nm}(R) = -\frac{\hbar^2}{2m} \sum_k G_{nk}^{-1}(R) \int_0^{\frac{\pi}{2}} d\alpha \phi_k^*(R, \alpha) \frac{\partial^2}{\partial R^2} \phi_m(R, \alpha). \quad (46)$$

Note, the coupling potentials differ only by the order of the derivative with respect to the hyperradius  $R$ . Most importantly the hyperspherical channel potential  $V_n(R)$  is given by

$$V_n(R) = [\lambda_n(R) - 4] \frac{\hbar^2}{2mR^2}. \quad (47)$$

We finally disentangled the hyperangle and radial components and end up with the two equations (42) and (44) which are only functions of one variable each. In particular the derivation of the channel potentials  $V_n(R)$ , which represent effective scattering potentials, require only the solution of an equation in the single variable  $\alpha$ . In contrast, the direct solution of the three-body Schrödinger equation using hyperspherical coordinates requires the solution of an equation of five variables [4]. The prize to pay here is the integro-differential structure of Eq. (42) which makes its solution more complicated. It turns out, however, that analytical solutions are still possible and even in the case where Eq. (42) does not provide analytical solutions, it can be solved using standard numerical techniques.

We are interested in the regime of resonant interactions,  $a \gg r_0$ , with energies  $E \approx 0$  close to the scattering threshold which we anticipate as the accumulation point of the Efimov states. At such low energies the Efimov states are very loosely bound and thus correspond to objects of large hyperradial extend. It turns out – and as we will (a posteriori) verify below – that the eigenvalues  $\lambda_n(R)$  are only very weakly dependent on the hyperradius  $R$  in this regime. This in turn implies that their corresponding eigenfunctions can only dependent weakly on  $R$ . Hence we may neglect *all* coupling terms  $P_{nm}$  and  $Q_{nm}$  in the hyperradial equation (44) because their magnitude is determined by the derivatives of  $\phi_n(R)$  with respect to  $R$  (This approximation is referred to as the “extended adiabatic hyperspherical approximation”).<sup>12</sup> The resulting radial equation has a remarkably simple form. It reads

$$\left[ \frac{\hbar^2}{2m} \left( -\frac{\partial^2}{\partial R^2} + \frac{15}{4R^2} \right) + V_n(R) \right] f_n(R) \approx E f_n(R). \quad (48)$$

When inserting the channel potential one finds

---

<sup>12</sup> In the so-called *adiabatic hyperspherical approximation* one neglects only off-diagonal coupling terms  $P_{nm}$  and  $Q_{nm}$ .

$$\boxed{\frac{\hbar^2}{2m} \left[ -\frac{\partial^2}{\partial R^2} + \underbrace{\frac{\lambda_n(R) - 1/4}{R^2}}_{V_{\text{eff}}(R)} \right] f_n(R) \approx E f_n(R)} \quad (49)$$

This equation has the form of a radial Schrödinger equation describing the scattering of a single particle in an inverse square potential. The strength of the potential  $\lambda_n(R) - 1/4$  is determined as well as modified by the  $R$ -dependent eigenvalues  $\lambda_n(R)$ . Hence, before we can turn to standard textbooks of quantum mechanics for the solution of the scattering in an inverse square potential we have to determine the eigenvalues  $\lambda_n(R)$ .

## VI. SOLUTION OF THE EIGENVALUE EQUATION

In order to determine the structure of the eigenvalues  $\lambda_n(R)$  we have to solve Eq. (42) in the appropriate regimes of interest. For convenience we display Eq. (42) again:

$$\left[ -\frac{\partial^2}{\partial \alpha^2} - \lambda_n(R) \right] \phi_n(R, \alpha) = -\frac{2mR^2}{\hbar^2} V(\sqrt{2}R \sin \alpha) \left[ \phi_n(R, \alpha) + \frac{4}{\sqrt{3}} \int_{\alpha_H}^{\alpha_L} \phi_n(R, \alpha') d\alpha' \right]. \quad (50)$$

where  $\alpha_H = \pi/2 - |\pi/6 - \alpha|$  and  $\alpha_L = |\pi/3 - \alpha|$ . We are interested in the ‘fluffy’, that is weakly bound Efimov states which are close to unitarity. Thus, since the hyperradius  $R$  determines the spatial extend of the trimer states, we are interested in the regime of large hyperradii  $R$ . At this point we recall that at fixed hyperradius  $R$  the hyperangle  $\alpha$  determines the relative magnitude of  $\mathbf{r}_{i,jk}$  and  $\mathbf{r}_{jk}$  via Eq. (26). The dependence of the hyperangle on  $r_{i,jk}$  and  $r_{jk}$  is illustrated in Fig. 9. For a small hyperangle  $\alpha \approx 0$  the atoms 2 and 3 are very close by while for  $\alpha$  approaching the opposite endpoint  $\alpha = \pi/2$  all three particles are guaranteed to be far away from each other when the hyperradius is large.

This allows a simple analysis of Eq. (50) for the regime of large, fixed hyperradius  $R$ . When  $r = R \sin \alpha \sim r_{23} \gg r_0$  is large enough (see Fig. 9(a), configuration to the right) we can neglect the two-body potential  $V(r)$  and Eq. (50) becomes

$$\left[ -\frac{\partial^2}{\partial \alpha^2} - \lambda_n \right] \phi_n(\alpha) = 0 \quad (51)$$

which is independent of  $R$ . Using the boundary condition  $\phi_n(\alpha = \pi/2) = 0$ , the solution to Eq. (51) is given by

$$\phi_n^{(\text{hi})}(R, \alpha) \approx \sin \left[ \lambda_n(R)^{1/2} \left( \frac{\pi}{2} - \alpha \right) \right]. \quad (52)$$

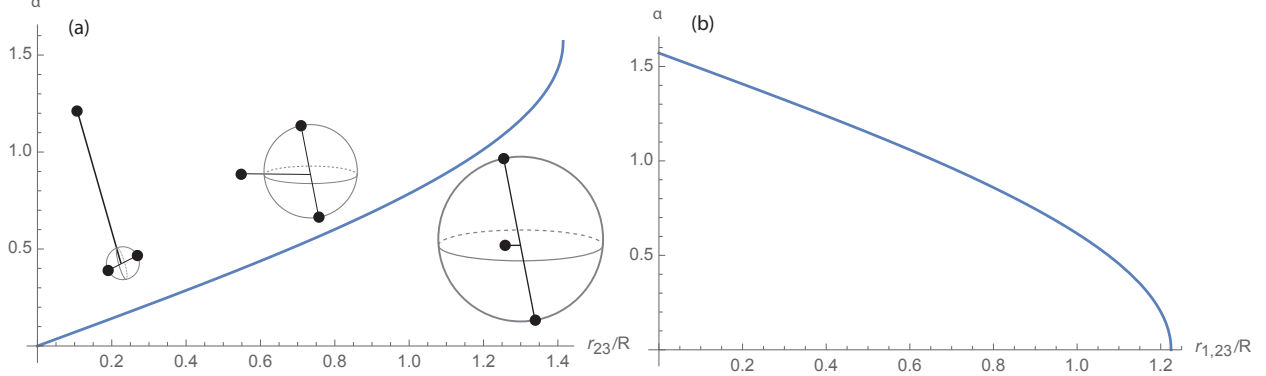


Figure 9: Dependence of the hyperangle  $\alpha$  on the magnitudes of  $\mathbf{r}_{i,jk}$  and  $\mathbf{r}_{jk}$  at fixed hyperradius  $R$ .

where  $\lambda_n(R)^{1/2} = 2(n + 1)$ .<sup>13</sup>

Further progress can be made in the regime where  $\alpha \rightarrow 0$ . In this regime fortunately the integral in Eq. (50) becomes traceable. For small  $\alpha$  we can resolve the absolute values in the bounds of the integral  $\alpha_H = \pi/3 + \alpha$  and  $\alpha_L = \pi/3 - \alpha$ . In the case of very small  $\alpha$  the region over which the integral is taken is limited to a small interval around  $\alpha' = \pi/3$ . Therefore the configuration  $\phi_n(\alpha' = \pi/3)$  is singled out in the integrand and which can be treated as constant in the small interval of size  $2\alpha \rightarrow 0$ . Furthermore we recall that we are interested in the regime of large  $R$  so that  $r = R \sin(\pi/3)$  is large compared to the range  $r_0$  of the two-body potential. In consequence, the  $\phi_n(\alpha')$  inside the integral is given by the solution  $\phi_n^{(hi)}$  from Eq. (52). Thus the angular Faddeev equation for small  $\alpha$  becomes,<sup>14</sup>

$$\left[ -\frac{\partial^2}{\partial \alpha^2} + \frac{2mR^2}{\hbar^2} V(\sqrt{2}R\alpha) \right] \phi_n^{(lo)}(R, \alpha) \approx -\frac{2mR^2}{\hbar^2} V(\sqrt{2}R\alpha) \frac{8\alpha}{\sqrt{3}} \phi_n^{(hi)}(R, \frac{\pi}{3}). \quad (53)$$

A particular solution to this inhomogeneous differential equation is given by

$$\phi_n^{(lo)}(R, \alpha) = -\frac{8\alpha}{\sqrt{3}} \phi_n^{(hi)}(R, \frac{\pi}{3}). \quad (54)$$

<sup>13</sup> The boundary condition  $\phi_n(\alpha = \pi/2) = 0$  enforces that in  $\psi(R, \alpha \approx \pi/2)$  given by Eq. (41) the term  $\sim \phi_n(R, \alpha)/\sin(2\alpha) \rightarrow (-1)^n(n + 1)$  so that the boundary condition at large  $R$  is purely determined by the hyperradial wavefunction  $f_n(R)$ .

<sup>14</sup> Note, that for brevity we neglected the eigenvalue  $\lambda_n(R)$  in the derivation. The eigenvalue  $\lambda_n(R)$  can easily be kept in the calculation as it formally only leads to a shift of the two-body potential. This shift converges to zero in the regime of  $R \gg r_0$ .

To construct the general solution of Eq. (55) we need the solution to the homogenous equation

$$\left[ -\frac{\partial^2}{\partial \alpha^2} + \frac{2mR^2}{\hbar^2} V(\sqrt{2}R\alpha) \right] \phi_n^{(lo)}(R, \alpha) \approx 0. \quad (55)$$

and which is analogous to the radial Schrödinger equation of two particle interacting at low scattering energies via a spherically symmetric potential  $V(\sqrt{2}R\alpha)$ . It is at this point of the calculation where the two-body physics and with it the scattering length  $a$  enters the problem. Let us denote the solution of this equation by  $\psi_0(r)$ . The general solution of the angular Faddeev equation in the regime of small  $\alpha \ll 1$ , Eq. (55), is then

$$\phi_n^{(lo)}(R, \alpha) \approx C(R)\psi_0(\sqrt{2}R\alpha) - \frac{8\alpha}{\sqrt{3}}\phi_n^{(hi)}(R, \frac{\pi}{3}), \quad (56)$$

where  $C(R)$  is a undetermined function of  $R$ .

### A. Efimov equation

Eq. (56) holds for  $\alpha \ll 1$  which, however, does not prevent us from choosing a large hyperradius  $R$  so that at the same time also  $R\alpha \gg r_0$  is fulfilled. Having this in mind,  $\psi_0(r)$  in Eq. (56) determined in the regime  $R \gg r_0$ : at large distances of atoms 2 and 3 given by  $R\alpha \gg r_0$  the wave function  $\psi_0(r)$  is simply given by the standard expression for the scattering wave function for short-range interactions [see for example Sakurai Eq. (7.7.10)]:

$$\psi_0(r) = \text{const}(r - a) \quad (57)$$

where  $a$  is the scattering length, the single parameter universally characterizing the underlying two-body potential. Here universality enters the calculation since the wave function in Eq. (57) is the same for any kind of short-range interaction.

As a next step one matches the high- $\alpha$  and low- $\alpha$  solutions given by Eq. (52) and (56). Here one takes advantage of the fact that the high- $\alpha$  solution which is an analytical function of  $\alpha$  can be extrapolated to low  $\alpha$  to match Eq. (56). The matching of the wave function values at  $\alpha = 0$  determines the coefficient  $C(R)$ . Comparing the derivatives with respect to  $\alpha$  at  $\alpha = 0$  yields an equation which determines the eigenvalues  $\lambda_n$ . It is given by Efimov's equation

$$\cos\left(\frac{\pi}{2}\lambda^{\frac{1}{2}}\right) - \frac{8}{\sqrt{3}}\lambda^{-\frac{1}{2}}\sin\left(\frac{\pi}{6}\lambda^{\frac{1}{2}}\right) = \sqrt{2}\lambda^{-\frac{1}{2}}\sin\left(\frac{\pi}{2}\lambda^{\frac{1}{2}}\right)\frac{R}{a}, \quad (58)$$

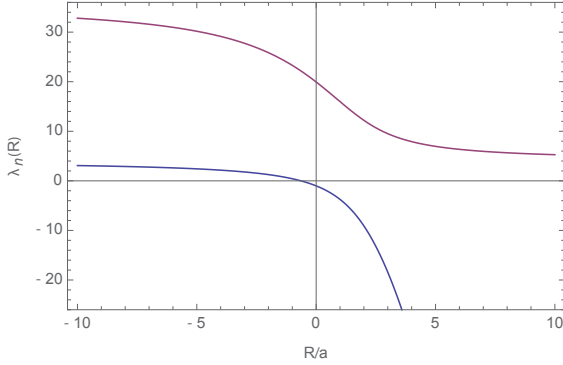


Figure 10: The lowest two eigenvalue solutions to Eq. (58) as function of the dimensionless variable  $R/a$ .

which we already encountered in the previous part of this lecture. It was first derived by Efimov in 1970 [14]. It lies at the heart of the Efimov effect, since it determines the strength of the effective hyperspherical scattering potentials  $V_n(R)$  in Eqn. (48) and (49). As we will see below, the strength of these inverse square potentials determines if one deals with the situation of an effective fall to the center problem (Efimov effect) or the absence of bound states.

## VII. THE EFIMOV EFFECT

At a given scattering length  $a$ , the Efimov equation (58) has infinitely many solutions for each choice of  $R$ . In Fig. 10 we show the lowest two solutions of Eq. (58) as function of the dimensionless variable  $R/a$ . Only the lowest eigenvalue  $\lambda_0(R)$  leads to an attractive channel potential  $V_n(R)$  given by Eq. (47). For this reason we will only consider the case  $n = 0$  ( $\lambda \equiv \lambda_0$ ). The eigenvalue  $\lambda_0(R/a)$  crosses over from 4 to  $-\infty$  as one goes from the “BCS” to the “BEC” side of the Feshbach resonance.

At unitarity,  $a = \infty$  we find the numerical value

$$s_0 \equiv \sqrt{|\lambda_0(0)|} = 1.00624\dots \quad (59)$$

which is the famous Efimov number  $s_0$ . Expanded around unitarity one finds

$$\lambda_0(R) \approx -s_0^2 \left( 1 + 1.897 \frac{R}{a} + \dots \right). \quad (60)$$

In consequence, something peculiar happens as one sits exactly at the resonance position where  $a = \infty$ : the eigenvalue  $\lambda_0(R)$  becomes completely independent of  $R$ . This justifies

a posteriori the extended adiabatic hyperspherical approximation, since the eigenvalues  $\lambda_n$  and with them their eigenfunctions  $\phi_n(R)$  become independent of  $R$ . In consequence the derivatives in Eqn. (45) and (46) vanish and thus the couplings  $P_{nm}$  and  $Q_{nm}$  are indeed zero. The  $R$ -independence of  $\lambda_0$  also implies that the effective scattering potential  $V_0(R)$  in Eq. (49) becomes a pure inverse square potential. The inverse square potential is a scale invariant potential<sup>15</sup> so that the three-body radial equation (49) describes scale invariant physics. Hence one would naively expect that the three-body problem preserves the scale invariance of the underlying two-body physics!

However, to see whether this is indeed the case we have to first solve quantum mechanics described by the hyperradial equation (49), which at unitarity can be written as

$$\frac{\hbar^2}{2m} \left[ -\frac{\partial^2}{\partial R^2} - \frac{s_0^2 + 1/4}{R^2} \right] f_0(R) = 0. \quad (61)$$

The potential has a divergence at  $R = 0$ . As we will see below this divergency is responsible for the emergence of infinitely deeply bound trimer states which is termed the Thomas effect and which is unphysical (cf. Fig. (4)). In fact for realistic two-body potentials the finite range  $r_0$  leads to a short distance repulsive core in the three-body potential which regularizes the divergent potential at  $R = 0$ . In consequence only a finite number of deeply bound states remains.

We are now left with the problem of analyzing the bound state solutions of Eq. (61) which correspond to three-body bound states. Recognizing that this equation corresponds to the simple scattering of a particle off an inverse square potential, let us briefly recall the physics of this problem.

### Recap: Inverse square potential scattering

Let us briefly summarize the quantum mechanics of the scattering of an inverse square potential [33]. Consider the radial Schrödinger equation of the scattering via the potential

$$U(r) = \frac{\hbar^2}{2m} \frac{\gamma}{r^2}, \quad (62)$$

---

<sup>15</sup>  $\frac{\hbar^2}{2m} \frac{1}{r^2}$  carries already the dimension of energy so that any proportionality coefficient is dimensionless. Thus no scale can be introduced by this coefficient and the system is scale invariant.

which is given by

$$-\frac{d^2 u_l(r)}{dr^2} + \frac{l(l+1) + \gamma}{r^2} u_l(r) = k^2 u_l(r). \quad (63)$$

For our analysis of Eq. (61) we are interested only in the limit of small  $k \rightarrow 0$  and  $l = 0$ . The two linear independent solutions are (as well known from the problem of two free particles)

$$u_{l_\gamma}(kr) = \sqrt{\frac{\pi}{2}} kr J_{l_\gamma + \frac{1}{2}}(kr), \quad v_{l_\gamma}(kr) = -\sqrt{\frac{\pi}{2}} kr Y_{l_\gamma + \frac{1}{2}}(kr) \quad (64)$$

with the ordinary Bessel functions  $J$  and  $Y$  and where one defines  $l_\gamma$  by  $\gamma \equiv l_\gamma(l_\gamma + 1)$ .

There is a critical interaction strength

$$\gamma_c = -\frac{1}{4} \quad (65)$$

which separates two distinct regimes of solutions. In the so-called under-critical regime where  $\gamma > \gamma_c$  the order of the Bessel functions is real and it can be shown [33] that only scattering states exist.

Contrarily, in the over-critical regime,  $\gamma < \gamma_c$  the order of the Bessel functions becomes imaginary:

$$l_\gamma + \frac{1}{2} = \sqrt{\frac{1}{4} + \gamma} \equiv i\tau, \quad \tau = \sqrt{|\gamma| - \frac{1}{4}} \quad (66)$$

In this case, the radial Schrödinger equation (63) supports scattering as well as bound state solutions. We are interested here in the latter which have the form

$$u_\tau(\kappa r) = \sqrt{\frac{\pi}{2}} \kappa r K_{i\tau}(\kappa r). \quad (67)$$

$K$  denotes the modified Bessel function and we defined the bound state wave number  $\kappa$  by the binding energy  $E_B = -\hbar^2 \kappa^2 / m$ . It is instructive to consider the limit of large  $r$ ,

$$u_\tau(\kappa r) \rightarrow e^{-\kappa r}, \quad (68)$$

which verifies that the wave function indeed fulfills correct (bound state) boundary condition. Interestingly, Eq. (67) represents a solution for *any* value of  $\kappa$  which is reminiscent of the underlying scale invariant Hamiltonian. However, we are dealing with a Hermitian problem and different solutions must be orthogonal to each other. It can be shown that this leads to the condition

$$\sin \left[ \tau \ln \left( \frac{\kappa_1}{\kappa_2} \right) \right] = 0 \quad (69)$$

where  $\kappa_{1/2}$  denote two distinct eigenvalues of Eq. (63). This condition directly implies a *discrete* bound state spectrum. By taking an arbitrary wave vector  $\kappa_*$  as reference scale we obtain an infinite series of bound states determined by the condition

$$\tau \ln \frac{\kappa_*}{\kappa_n} = n\pi \quad \Rightarrow \quad E_n = E_* e^{-2\pi n/\tau} \quad n = 1, 2, 3, \dots . \quad (70)$$

Expressed differently the bound states obey a geometrical spectrum given by

$$\frac{E_{n+1}}{E_n} = e^{-2\pi/\tau}. \quad (71)$$


---

This result is now easily applied to the three body problem and we finally are able to derive the Efimov effect.

In our case  $\gamma = -s_0^2 - 1/4 = -1.2625\dots$  so that we are safely in the over-critical regime. Furthermore,  $\tau = s_0$  and thus our calculation predicts the infinite series of Efimov states at  $a = \infty$  which obey the geometric spectrum

$$\frac{E_{n+1}}{E_n} = e^{-2\pi/s_0} \approx 515.035 \quad (72)$$

with accumulation point at  $E = 0$ . Thus we have finally derived the existence of the Efimov effect recovering the discrete scaling law of energies already presented in Eq. (13). As mentioned above the calculation also predicts the existence of infinitely many deeply bound trimer states as the spectrum given by Eq. (72) is not bounded from below. This is of course unphysical and the problem is resolved by corrections to the hyperspherical potential  $V_{\text{eff}}(R)$  at small hyperradius  $R$ .

Finally we may rise the question, what the spectrum at finite scattering length away from unitarity looks like? Keeping explicitly the scattering length in the previous calculation shows that the hyperspherical potential is exponentially cut off at distances  $R \approx |a|$ . As a decreasing is magnitude from  $a = \infty$  this extinguishes, one by one, each of the Efimov trimer bound states until finally, when  $|a| \approx r_0$  – here the inclusion the physical modifications at small  $R$  is crucial – no trimer bound state is left. Although this is in principle a relatively straightforward task it can be tedious in detail and is beyond the scope of this lecture. Although we do not calculate a full Efimov spectrum in these lecture notes we show for completeness in Fig. 11(a) a predicted Efimov spectrum, calculated for a realistic two-channel Feshbach resonance model of arbitrary resonance strength  $s_{\text{res}}$ . The model includes

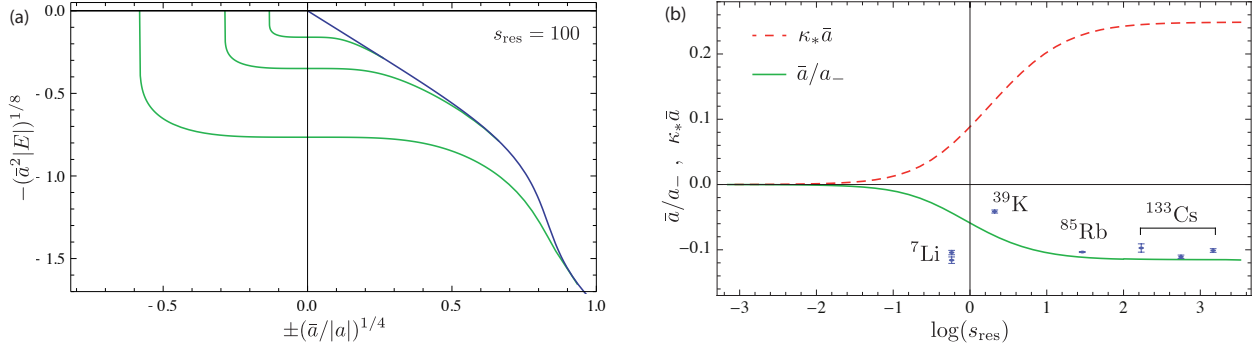


Figure 11: (a) Efimov spectrum as calculated exactly using a functional renormalization group approach for a realistic two-channel Feshbach resonance model of strength  $s_{\text{res}} = 100$  (see previous lectures on the Feshbach resonance model) which featured additionally a finite range  $\bar{a}$  of the open to closed-channel coupling set by the van-der Waals range [13]. (b) Scattering length  $a_-$  where the first/lowest Efimov state reaches the scattering continuum as function of the resonance strength.

a finite range of the open to closed-channel coupling which is set by the van-der Waals range [13]. In Fig. 11(b) we show the predicted scattering length  $a_-$  where the first/lowest Efimov state reaches the scattering continuum and the comparison to experimental measurements.

Having derived in detail the existence of the Efimov effect we now turn briefly to the question of how the Efimov effect can be observed using ultracold atoms.

## VIII. EXPERIMENTAL OBSERVATION OF THE EFIMOV EFFECT USING COLD ATOMS

Basically there are two experimental routes which have been taken to reveal Efimov physics with cold atoms. The ‘standard’ approach is an indirect detection by measuring three-body loss enhancements caused by Efimov physics. The other approach is the direct photo association of Efimov trimers using radio-frequency spectroscopy. In the former approach one exploits the instability of cold atomic gases caused by the recombination of atoms into deep molecular bound states. The binding energy gained in the formation of a molecule is transferred into kinetic energy of the atoms participating in the process. When this energy exceeds the trap depth, the atoms have sufficient momentum to escape from the trapping potential. Having escaped from the trap, these atoms are obviously not present

in a subsequent absorption image, by which the number of trapped atoms is determined experimentally. By measuring the remaining fraction of atoms as function of time the loss rate can then be inferred.

As discussed in a previous lecture, in order for momentum to be a conserved quantity, such collisional loss processes have to involve at least three atoms.<sup>16</sup> The third atom ensures momentum conservation by carrying away a portion of the binding energy released in the recombination process. Since three atoms are involved, the loss rate is proportional to the third power of density [34],

$$\dot{n} = -K_3 n^3, \quad (73)$$

where  $K_3$  is the three-body loss coefficient and  $n$  the density of atoms. As mentioned before, the existence of loss processes in ultracold atomic gases is quite natural: after all, the true ground state of the system is not the gas of atoms but a solid – with the exception of the helium where the atoms would form a liquid. In consequence, ultracold gases are in a metastable state and the loss process discussed above is one of the many ways by which the system can reach its true ground state.

Let us now briefly discuss three observables which are related to three-body decay and which can be used to detect Efimov physics.

**Three-atom recombination maxima for  $a < 0$ .** The first possibility to find evidence for Efimov states is the measurement of the loss coefficient  $K_3$  in dependence of negative scattering length  $a$ . In the scaling limit, cf. Eq. (17),  $K_3$  can be expressed as [4]

$$K_3 = 3C(a) \frac{\hbar^2 a^4}{m}. \quad (74)$$

When no Efimov state is present, one finds a pure  $a^4$  scaling with a constant coefficient  $C(a)$ . This scaling is due to the process schematically shown in Fig. 12(a), where two atoms form a virtual scattering state (dashed line). This state subsequently interacts with a third atom (dashed vertex). The outgoing, deeply bound molecule as well as the outgoing atom can be ‘on-shell’, physical scattering states. The evaluation of the corresponding matrix element yields Eq. (74).

---

<sup>16</sup> Two-body decay processes are also possible. These can, however, be often made sufficiently small in order to be neglected.

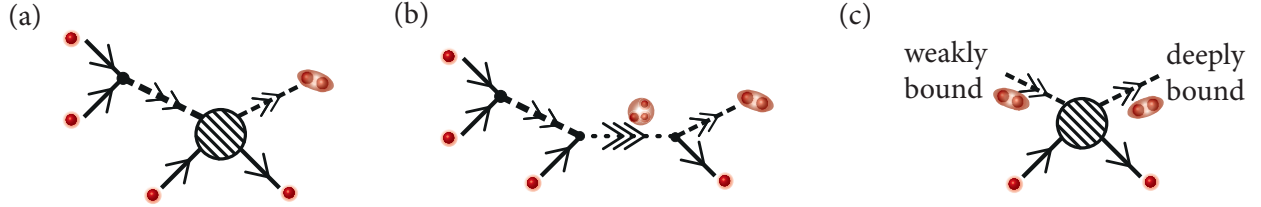


Figure 12: Collisional processes leading to three-body decay of ultracold atomic gases. Solid lines represent atoms, dashed lines molecules and dotted lines with three arrows Efimov trimers. (a) Three-atom recombination. (b) In the presence of a trimer a new decay channel opens up. (c) Atom-dimer recombination at the atom-dimer scattering threshold.

The situation changes, when an Efimov state is nearby or even crosses the atom scattering threshold at the scattering length  $a$  where the measurement is performed. In this case a new, fast decay channel opens up. The new process contributing to Fig. 12(a) is schematically depicted in Fig. 12(b). When the third atom enters, a new state, the trimer, can be formed. This trimer has typically a very short lifetime and it decays quickly into deeply bound states. Furthermore, when the trimer is energetically close to the atom threshold at zero energy, it is almost gapless and thus the corresponding matrix element becomes very large. This leads to a large enhancement of the loss which is visible as a resonance in  $K_3 = K_3(a)$ .

This additional modification due to Efimov physics is described by the scattering length dependent prefactor  $C(a)$  in Eq. (74), which, in the resonance limit, has to obey  $C(22.7a) = C(a)$  due to the discrete scale invariance of Efimov physics. The loss process for  $a < 0$  was first discussed by Esry, Greene and Burke [35]. Using effective field theory, Braaten and Hammer derived an analytical expression for  $C(a)$  in the scaling limit [36]

$$C(a) = 4590 \frac{\sinh(2\eta_-)}{\sin^2[s_0 \ln(a/a_-)] + \sinh^2 \eta_-}. \quad (75)$$

Here  $a_-$  is a representative of the three-body parameter as described in the previous part of this lecture, and  $\eta_-$  reflects the finite lifetime of the trimer state involved. By fine-tuning the parameters  $a_-$  and  $\eta_-$ , Eq. (75) can be used to fit the experimental results. Three-body loss enhancements due to Efimov physics have been found in many cases [15, 37–46] and in Fig. 13 we show two examples. While in Fig. 13(a) the first measurement of an Efimov loss resonance for identical bosons [15] is shown, Fig. 13(b) displays the loss coefficient in a three-component  ${}^6\text{Li}$  Fermi gas [38] where the Efimov effect appears as well.

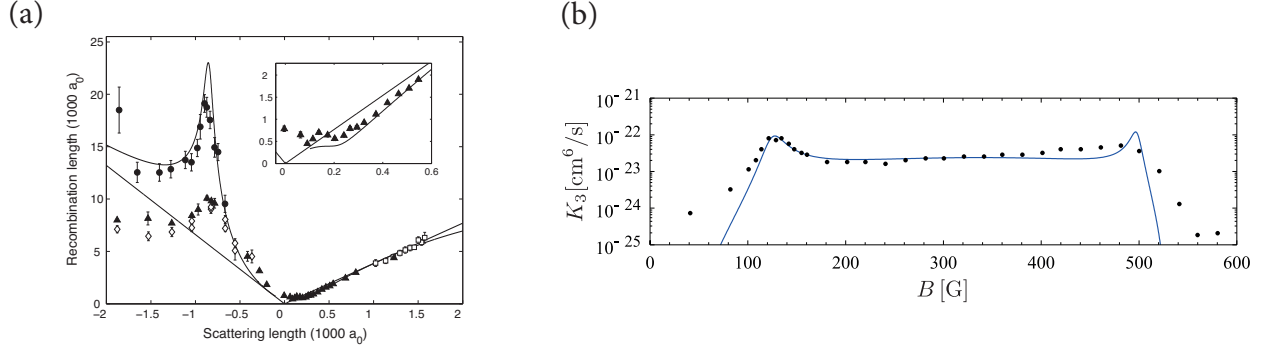


Figure 13: (a) First indirect observation of an Efimov trimer in a ultracold gas of  $^{133}\text{Cs}$  atoms. The measured recombination length (symbols) is shown versus the scattering length  $a$  and compares well with results from scaling theory (solid curve) [Figure taken from [15] by courtesy of R. Grimm]. (b) Three-body loss coefficient  $K_3$  as function of magnetic field in a three-component  $^6\text{Li}$  Fermi gas. The resonances are due to Efimov states. Experimental data from [38] (symbols) versus theory [47] (curve).

**Three-atom recombination minima for  $a > 0$ .** For  $a > 0$ , three atoms at the atom threshold at  $E = 0$ , cf. Fig. 3, can recombine into the weakly bound dimer state (green solid line in Fig. 3). In this case the two processes shown in Fig. 12(a) and (b) do not lead to enhancement but rather a reduction of losses, since both processes conspire in such a way that the corresponding matrix elements interfere destructively with each other. In the scaling limit, the corresponding coefficient  $C(a)$  obeys the equation [4]

$$C(a) = 67.1 e^{-2\eta_+} (\cos^2[s_0 \ln(a/a_+)] + \sinh^2 \eta_+) + 16.8 (1 - e^{-4\eta_+}). \quad (76)$$

Similarly to Eq. (75),  $a_+$  is a possible representative of the three-body parameter and  $\eta_+$  determines the lifetime of the trimer responsible for the minimum. Recombination minima were for instance observed in [15], cf. Fig. 13(a, inset). The existence of these minima may become of great importance for many-body physics as they might help to stabilize strongly interacting repulsive Bose or  $SU(N)$  Fermi gases for  $a/r_0 \gg 1$ .

**Loss resonances in atom-dimer scattering.** It is also possible to prepare a mixture of weakly bound dimers and free atoms in which both constituents interact with each other. During this process, depicted in Fig. 12(c), the weakly bound dimer can fall into a deeply bound molecular state and the participating atoms leave the trap. Similar to the discussion

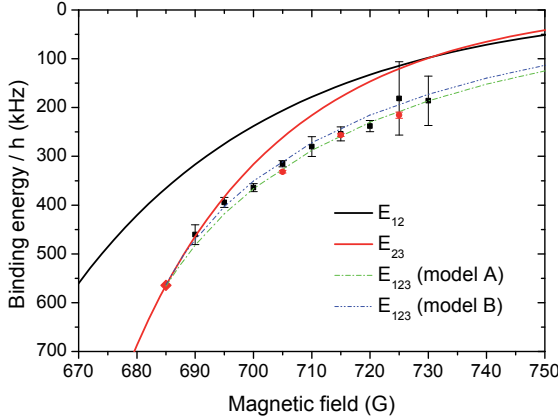


Figure 14: Energies of Efimov trimers as measured by direct association using rf spectroscopy (data points). The formation of the Efimov states is performed close to the atom-dimer threshold (red solid line). The figure is taken from [50].

below Eq. (74), a close-by trimer state leads to an enhanced loss and the corresponding loss rate is parametrized by [48]<sup>17</sup>

$$\dot{n}_D = \dot{n}_A = -\beta(a)n_Dn_A. \quad (77)$$

In the scaling limit, the coefficient  $\beta$  has the form

$$\beta(a) = C_{AD}(a) \frac{\hbar a}{m}, \quad (78)$$

with

$$C_{AD}(a) = 20.3 \frac{\sinh(2\eta_*)}{\sin^2[s_0 \ln(a/a_*)] + \sinh^2 \eta_*}, \quad (79)$$

and where again,  $a_*$  and  $\eta_*$  are representatives of the three-body parameter and the lifetime of the trimer, respectively. The enhanced atom-dimer loss has been studied experimentally for instance in [48, 49]. Note that in the case of  $a > 0$ , non-universal corrections become particularly important, as the atom-dimer threshold itself (green solid line in Fig. 3) exhibits a strong dependence on microscopic details when  $a$  becomes of the order of  $r_0$ .

**Photo association of trimers.** Let us conclude this lecture note by the last possible route taken to detect Efimov physics. Here one does not rely on a indirect measurement

<sup>17</sup> Here we neglect dimer-dimer scattering as well as the three-atom recombination also present in these mixtures.

but directly associates the Efimov trimers. Recently the group of Jochim succeeded to use radio-frequency (rf) modulations to associate trimers from a mixture of atoms and dimers in an two-component mixture of  ${}^6\text{Li}$  atoms [50], see Fig. 14. By applying an rf pulse, one hyperfine spin is flipped and a trimer is associated in the final state. By measuring the rf response it was then possible to directly determine the binding energy of the Efimov bound state, which is, however, a very short-lived state. Similar results have been reported in [39, 51].

---

- [1] W. Ketterle and M. W. Zwierlein, in *Ultracold Fermi Gases Proceedings of the International School of Physics ‘Enrico Fermi’, Course CLXIV, Varenna 2006*, edited by M. Inguscio, W. Ketterle, and S. C. (IOS Press, Amsterdam, 2008).
- [2] N. W. Ashcroft and N. D. Mermin, *Solid State Physics* (Brooks/Cole, Belmont, 1976).
- [3] G. Baym and C. Pethick, Annual Review of Astronomy and Astrophysics **17**, 415 (1979).
- [4] E. Braaten and H.-W. Hammer, Physics Reports **428**, 259 (2006), ISSN 0370-1573, URL <http://www.sciencedirect.com/science/article/pii/S0370157306000822>.
- [5] R. Schmidt, Ph.D. thesis, München, Technische Universität München, Diss., 2013 (2013).
- [6] L. Landau and E. Lifshitz, *Quantum Mechanics* (Butterworth-Heinemann, Oxford, UK, 1980).
- [7] S. Sachdev, *Quantum Phase Transitions* (Cambridge University Press, 2000).
- [8] S. Sachdev, in *BCS–BEC Crossover and the Unitary Fermi Gas*, edited by W. Zwerger (Lecture Notes in Physics, Springer, 2012).
- [9] M. J. H. Ku, A. T. Sommer, L. W. Cheuk, and M. W. Zwierlein, Science **335**, 563 (2012), URL <http://www.sciencemag.org/content/335/6068/563.abstract>.
- [10] G. Zürn, T. Lompe, A. N. Wenz, S. Jochim, P. S. Julienne, and J. M. Hutson, Phys. Rev. Lett. **110**, 135301 (2013), URL <http://link.aps.org/doi/10.1103/PhysRevLett.110.135301>.
- [11] W. Zwerger, ed., *BCS–BEC Crossover and the Unitary Fermi Gas* (Lecture Notes in Physics, Springer, 2012).
- [12] A. Gezerlis and J. Carlson, Phys. Rev. C **77**, 032801 (2008), URL <http://link.aps.org/doi/10.1103/PhysRevC.77.032801>.
- [13] R. Schmidt, S. Rath, and W. Zwerger, The European Physical Journal B **85**, 1 (2012), ISSN 1434-6028, URL <http://dx.doi.org/10.1140/epjb/e2012-30841-3>.

- [14] V. Efimov, Physics Letters B **33**, 563 (1970), ISSN 0370-2693, URL <http://www.sciencedirect.com/science/article/pii/0370269370903497>.
- [15] T. Kraemer, M. Mark, P. Waldburger, J. G. Danzl, C. Chin, B. Engeser, A. D. Lange, K. Pilch, A. Jaakkola, H. C. Naegerl, et al., Nature **440**, 315 (2006), URL <http://dx.doi.org/10.1038/nature04626>.
- [16] T. K. Lim, K. Duffy, and W. C. Damer, Phys. Rev. Lett. **38**, 341 (1977), URL <http://dx.doi.org/10.1103/PhysRevLett.38.341>.
- [17] R. Brühl, A. Kalinin, O. Kornilov, J. P. Toennies, G. C. Hegerfeldt, and M. Stoll, Phys. Rev. Lett. **95**, 063002 (2005), URL <http://link.aps.org/doi/10.1103/PhysRevLett.95.063002>.
- [18] R. Amado and J. Noble, Physics Letters B **35**, 25 (1971), ISSN 0370-2693, URL <http://www.sciencedirect.com/science/article/pii/0370269371904291>.
- [19] R. D. Amado and J. V. Noble, Phys. Rev. D **5**, 1992 (1972), URL <http://link.aps.org/doi/10.1103/PhysRevD.5.1992>.
- [20] V. Efimov, Sov. J. Nucl. Phys. **29**, 546 (1979).
- [21] L. H. Thomas, Phys. Rev. **47**, 903 (1935), URL <http://link.aps.org/doi/10.1103/PhysRev.47.903>.
- [22] K. G. Wilson, Phys. Rev. D **3**, 1818 (1971), URL <http://link.aps.org/doi/10.1103/PhysRevD.3.1818>.
- [23] S. Moroz, S. Floerchinger, R. Schmidt, and C. Wetterich, Phys. Rev. A **79**, 042705 (2009), URL <http://link.aps.org/doi/10.1103/PhysRevA.79.042705>.
- [24] D. T. Son, Phys. Rev. Lett. **98**, 020604 (2007), URL <http://link.aps.org/doi/10.1103/PhysRevLett.98.020604>.
- [25] Y. Castin, Comptes Rendus Physique **5**, 407 (2004), ISSN 1631-0705, URL <http://www.sciencedirect.com/science/article/pii/S1631070504000866>.
- [26] V. Efimov, Sov. Phys. JETP Lett. p. 34 (1972).
- [27] E. Nielsen, D. Fedorov, A. Jensen, and E. Garrido, Physics Reports **347**, 373 (2001), ISSN 0370-1573, URL <http://www.sciencedirect.com/science/article/pii/S0370157300001071>.
- [28] S. Floerchinger, S. Moroz, and R. Schmidt, Few-Body Systems **51**, 153 (2011), ISSN 0177-7963, URL <http://dx.doi.org/10.1007/s00601-011-0231-z>.

- [29] D. Fedorov and A. Jensen, Physical review letters **71**, 4103 (1993).
- [30] S. I. Vinitskii, V. S. Melezhik, L. I. Ponomarev, I. V. Puzynin, T. P. Puzynina, L. N. Somov, and N. F. Truskova, Soviet Journal of Experimental and Theoretical Physics **52**, 353 (1980).
- [31] L. Faddeev, JETP (Sov. Phys.) **12**, 216 (1961).
- [32] V. Efimov, Sov. J. Nucl. Phys. **12**, 101 (1971).
- [33] H. Friedrich, ed., *Scattering Theory*, vol. 872 of *Lecture Notes in Physics*, Berlin Springer Verlag (2013).
- [34] L. P. Pitaevskii and S. Stringari, *Bose-Einstein Condensation* (Oxford University Press, 2003).
- [35] B. D. Esry, C. H. Greene, and J. P. Burke, Phys. Rev. Lett. **83**, 1751 (1999), URL <http://link.aps.org/doi/10.1103/PhysRevLett.83.1751>.
- [36] E. Braaten and H.-W. Hammer, Phys. Rev. Lett. **87**, 160407 (2001), URL <http://link.aps.org/doi/10.1103/PhysRevLett.87.160407>.
- [37] M. Berninger, A. Zenesini, B. Huang, W. Harm, H.-C. Nägerl, F. Ferlaino, R. Grimm, P. S. Julienne, and J. M. Hutson, Phys. Rev. Lett. **107**, 120401 (2011), URL <http://link.aps.org/doi/10.1103/PhysRevLett.107.120401>.
- [38] T. B. Ottenstein, T. Lompe, M. Kohnen, A. N. Wenz, and S. Jochim, Phys. Rev. Lett. **101**, 203202 (2008), URL <http://link.aps.org/doi/10.1103/PhysRevLett.101.203202>.
- [39] O. Machtey, Z. Shotan, N. Gross, and L. Khaykovich, Phys. Rev. Lett. **108**, 210406 (2012), URL <http://link.aps.org/doi/10.1103/PhysRevLett.108.210406>.
- [40] J. H. Huckans, J. R. Williams, E. L. Hazlett, R. W. Stites, and K. M. O’Hara, Phys. Rev. Lett. **102**, 165302 (2009), URL <http://link.aps.org/doi/10.1103/PhysRevLett.102.165302>.
- [41] S. E. Pollack, D. Dries, and R. G. Hulet, Science **326**, 1683 (2009).
- [42] M. Zaccanti, B. Deissler, C. D’Errico, M. Fattori, M. Jona-Lasinio, S. Muller, G. Roati, M. Inguscio, and G. Modugno, Nature Physics **5**, 586 (2009).
- [43] N. Gross, Z. Shotan, S. Kokkelmans, and L. Khaykovich, Phys. Rev. Lett. **103**, 163202 (2009), URL <http://link.aps.org/doi/10.1103/PhysRevLett.103.163202>.
- [44] N. Gross, Z. Shotan, S. Kokkelmans, and L. Khaykovich, Phys. Rev. Lett. **105**, 103203 (2010), URL <http://link.aps.org/doi/10.1103/PhysRevLett.105.103203>.
- [45] R. J. Wild, P. Makotyn, J. M. Pino, E. A. Cornell, and D. S. Jin, Phys. Rev. Lett. **108**, 145305 (2012), URL <http://link.aps.org/doi/10.1103/PhysRevLett.108.145305>.
- [46] S. Roy, M. Landini, A. Trenkwalder, G. Semeghini, G. Spagnolli, A. Simoni, M. Fattori,

- M. Inguscio, and G. Modugno, arXiv:1303.3843 (2013).
- [47] S. Floerchinger, R. Schmidt, and C. Wetterich, Phys. Rev. A **79**, 053633 (2009), URL <http://link.aps.org/doi/10.1103/PhysRevA.79.053633>.
- [48] S. Knoop, F. Ferlaino, M. Mark, M. Berninger, H. Schobel, H. C. Nagerl, and R. Grimm, Nature Physics **5**, 227 (2009).
- [49] A. N. Wenz, T. Lompe, T. B. Ottenstein, F. Serwane, G. Zürn, and S. Jochim, Phys. Rev. A **80**, 040702 (2009).
- [50] T. Lompe, T. B. Ottenstein, F. Serwane, A. N. Wenz, G. Zürn, and S. Jochim, Science **330**, 940 (2010), URL <http://www.sciencemag.org/content/330/6006/940.abstract>.
- [51] S. Nakajima, M. Horikoshi, T. Mukaiyama, P. Naidon, and M. Ueda, Phys. Rev. Lett. **106**, 143201 (2011), URL <http://link.aps.org/doi/10.1103/PhysRevLett.106.143201>.